COMPUTER METHODS IN MATERIALS SCIENCE

2021, vol. 21, no. 1, 51–58
https://doi.org/10.7494/cmms.2021.1.0742

FFT-based simulation using a reduced set of frequencies adapted to the underlying microstructure

Christian Gierden[1*], Johanna Waimann[1], Bob Svendsen[2,3], Stefanie Reese[1]

[1] RWTH Aachen University, Institute of Applied Mechanics, 52074 Aachen, Germany.
[2] RWTH Aachen University, Material Mechanics, 52062 Aachen, Germany.
[3] Max-Planck-Institut für Eisenforschung GmbH, Microstructure Physics and Alloy Design, 40237 Düsseldorf, Germany.

Abstract

Instead of the classical finite element (FE) based microstructure simulation, a Fast Fourier transform (FFT) based microstructure simulation, introduced by Moulinec and Suquet (1994, 1998), also enables the computation of highly resolved microstructural fields. In this context, the microscopic boundary value problem is captured by the Lippmann–Schwinger equation and solved by using Fast Fourier transforms (FFT) and fixed-point iterations. To decrease the computational effort of the fixed-point solver, Kochmann et al. (2019) introduced a model order reduction (MOR) technique based on solving the Lippmann-Schwinger equation in Fourier space with a reduced set of frequencies. Thereby, the accuracy of this MOR technique depends on the number of used frequencies and the choice of frequencies that are considered within the simulation. Instead of the earlier proposed fixed (Kochmann et al., 2019) or geometrically adapted (Gierden et al., 2021b) sampling patterns, we propose a sampling pattern which is updated after each load step based on the current strain. To show the precision of such a strain-based sampling pattern, an elasto-plastic two-phase composite microstructure is investigated.

Keywords: microstructure simulation, FFT, model order reduction, composites

1. Introduction

The classical numerical two-scale simulation approach considering a spatially resolved microstructure is the FE^2 method (Smit et al., 1998). Within this simulation approach, the FE method is used to solve the macroscopic as well as the microscopic boundary value problem. Replacing the FE simulation on the microscale by a FFT-based simulation leads to the FE-FFT-based method (Kochmann et al., 2016; Spahn et al., 2014). Under periodic boundary conditions, the FFT-based simulation approach has proven to be more efficient than the FE-based simulation (Moulinec & Suquet, 1994; 1998). Thus, the FE-FFT-based method is a powerful alternative to the classical FE^2 method. Nevertheless, the high fidelity two-scale simulation of complex macroscopic boundary value problems is computationally very demanding for both methods.

To generate an efficient two-scale FE-FFT-based simulation approach for computing the overall material response, the microstructure might be coarsely discretized. Since this coarse discretization consequently only leads to inaccurate microstructural results, a subsequent post-processing step can be used to generate

* Corresponding author: christian.gierden@ifam.rwth-aachen.de
ORCID ID's: 0000-0003-1978-3570 (Ch. Gierden), 0000-0002-7579-7240 (J. Waimann), 0000-0002-1519-9433 (B. Svendsen), 0000-0003-4760-8358 (S. Reese)

high fidelity microstructural fields. Therefore, the macroscopic strain/deformation gradient of any macroscopic point of interest is saved during the entire simulation and applied to a fine discretized microstructure in the post-processing step (Gierden et al., 2021a; Kochmann et al., 2018). Other recently developed MOR techniques deal with a more precise approximation of the microstructure during the entire FFT-based simulation. These methods are, for example, based on a proper orthogonal decomposition (Garzcia-Cardona et al., 2017), low-rank approximations (Vondřejc et al., 2020) or a reduced set of frequencies (Kochmann et al., 2019).

The present paper concerns the MOR technique using a reduced set of frequencies. The accuracy of the applied MOR depends on the number and on the choice of considered frequencies. Therefore, Gierden et al. (2021b) presented a geometrically adapted sampling pattern to increase the precision of the initially introduced fixed, radial sampling pattern (Kochmann et al., 2019). To generate even more precise results in terms of nonlinear material behavior, we introduce the utilization of a strain-based sampling pattern. Based on the microstructural strain, this sampling pattern is redefined after each load step.

After briefly reviewing the FFT-based method in Section 2, the MOR technique based on a reduced set of frequencies is summed up in Section 3. Thereafter, the focus of this section lies on the definition of the strain-based sampling pattern. Section 4 shows the numerical results using this sampling pattern and compares the results to the earlier introduced sampling patterns. The paper ends with a conclusion and an outlook in Section 5.

2. FFT-based microstructure simulation

Considering an inhomogeneous periodic microstructure Ω, the microscopic boundary value problem (BVP) considering small strain kinematics yields:

$$\begin{aligned} &\operatorname{div} \boldsymbol{\sigma}(\bar{\boldsymbol{x}}, \boldsymbol{x}) = 0 \qquad \forall\, \boldsymbol{x} \in \Omega \\ &\boldsymbol{\sigma}(\bar{\boldsymbol{x}}, \boldsymbol{x}) = \boldsymbol{\sigma}(\bar{\boldsymbol{x}}, \boldsymbol{x}, \boldsymbol{\varepsilon}(\bar{\boldsymbol{x}}, \boldsymbol{x}), \boldsymbol{\alpha}(\boldsymbol{x})) \\ &\boldsymbol{\varepsilon}(\bar{\boldsymbol{x}}, \boldsymbol{x}) = \overline{\boldsymbol{\varepsilon}}(\bar{\boldsymbol{x}}) + \widetilde{\boldsymbol{\varepsilon}}(\boldsymbol{x}) \end{aligned} \tag{1}$$

Herein, the total microscopic strain $\boldsymbol{\varepsilon}(\bar{\boldsymbol{x}}, \boldsymbol{x})$ is additively split into a macroscopic part $\overline{\boldsymbol{\varepsilon}}(\bar{\boldsymbol{x}})$ at the macroscopic position $\bar{\boldsymbol{x}}$ and a microscopically influenced part $\widetilde{\boldsymbol{\varepsilon}}(\boldsymbol{x})$ at the microscopic position $\boldsymbol{x}$. The total stress $\boldsymbol{\sigma}(\bar{\boldsymbol{x}}, \boldsymbol{x})$ depends on the resulting total strain and some internal variables $\boldsymbol{\alpha}(\boldsymbol{x})$. In regard to comprehensibility, in the following, the dependence of all variables besides the macroscopic strains on the macroscopic position $\bar{\boldsymbol{x}}$ is not shown.

To capture an isotropic elasto-plastic material behavior, the total strain $\boldsymbol{\varepsilon}(\boldsymbol{x}) = \boldsymbol{\varepsilon}_e(\boldsymbol{x}) + \boldsymbol{\varepsilon}_p(\boldsymbol{x})$ is additively split into an elastic part $\boldsymbol{\varepsilon}_e(\boldsymbol{x})$ and a plastic part $\boldsymbol{\varepsilon}_p(\boldsymbol{x})$. The linear-elastic stress-strain relation reads $\boldsymbol{\sigma}(\boldsymbol{x}) = \mathbf{C}(\boldsymbol{x}) : \boldsymbol{\varepsilon}_e(\boldsymbol{x})$ with the isotropic stiffness tensor $\mathbf{C}(\boldsymbol{x})$. In terms of the classical von Mises yield condition with isotropic linear hardening, the yield condition has the form:

$$\Phi(\boldsymbol{\sigma}(\boldsymbol{x}), \varepsilon_p^{acc}(\boldsymbol{x}), \boldsymbol{x}) = \sigma^{eq}(\boldsymbol{x}) - [\sigma_y^{\,0}(\boldsymbol{x}) + H(\boldsymbol{x})\varepsilon_p^{acc}(\boldsymbol{x})] \tag{2}$$

with the initial yield stress $\sigma_y^{\,0}(\boldsymbol{x})$, the von Mises equivalent stress $\sigma^{eq}(\boldsymbol{x})$, the hardening modulus $H(\boldsymbol{x})$ and the accumulated plastic strain $\varepsilon_p^{acc}(\boldsymbol{x})$. The associative flow rule reads:

$$\boldsymbol{\varepsilon}_p = \dot{\gamma}\frac{\partial \Phi}{\partial \boldsymbol{\sigma}} \tag{3}$$

with the plastic multiplier $\dot{\gamma}$. Additionally, the Karush–Kuhn–Tucker conditions $\Phi \leq 0$, $\dot{\gamma} \geq 0$ and $\Phi\, \dot{\gamma} = 0$ need to be fulfilled.

Using the FFT-based method to solve the inhomogeneous BVP in Equation (1), this BVP is transferred into an equivalent homogeneous representation (Hashin & Shtrikman, 1962) by defining a homogeneous reference material behavior $\mathbf{C}^0$ and the polarization stress $\boldsymbol{\tau}(\boldsymbol{x})$, which represents the inhomogeneities within the microstructural material behavior:

$$\begin{aligned} &\operatorname{div} \mathbf{C}^0{:}\boldsymbol{\varepsilon}(\boldsymbol{x}) + \operatorname{div} \boldsymbol{\tau}(\boldsymbol{x}) = 0 \qquad \forall\, \boldsymbol{x} \in \Omega \\ &\boldsymbol{\tau}(\boldsymbol{x}) = \boldsymbol{\sigma}(\boldsymbol{x}, \boldsymbol{\varepsilon}(\boldsymbol{x}), \boldsymbol{\alpha}(\boldsymbol{x})) - \mathbf{C}^0{:}\boldsymbol{\varepsilon}(\boldsymbol{x}) \\ &\boldsymbol{\varepsilon}(\boldsymbol{x}) = \overline{\boldsymbol{\varepsilon}}(\bar{\boldsymbol{x}}) + \widetilde{\boldsymbol{\varepsilon}}(\boldsymbol{x}) \end{aligned} \tag{4}$$

Using Green's function $\boldsymbol{G}^0(\boldsymbol{x}, \boldsymbol{x}')$ and thus the Lippmann–Schwinger operator $\boldsymbol{\Gamma}^0(\boldsymbol{x}, \boldsymbol{x}')$ to solve the BVP yields the integral equation:

$$\boldsymbol{\varepsilon}(\boldsymbol{x}) = \overline{\boldsymbol{\varepsilon}}(\bar{\boldsymbol{x}}) - \int \boldsymbol{\Gamma}^0(\boldsymbol{x}, \boldsymbol{x}') : \boldsymbol{\tau}(\boldsymbol{x}')\, d\boldsymbol{x}' \tag{5}$$

which is known as the Lippmann-Schwinger equation (Kröner, 1959; Willis, 1981). Its transfer into Fourier space enables the calculation of the strain in the Fourier space $\hat{\boldsymbol{\varepsilon}}(\boldsymbol{\xi})$, which is then depending on the frequencies:

$$\hat{\boldsymbol{\varepsilon}}(\boldsymbol{\xi}) = \begin{cases} -\hat{\boldsymbol{\Gamma}}^0(\boldsymbol{\xi})\hat{\boldsymbol{\tau}}(\boldsymbol{\xi}) & \forall \quad \boldsymbol{\xi} = 0 \\ \overline{\boldsymbol{\varepsilon}} & \forall \quad \boldsymbol{\xi} \neq 0 \end{cases} \tag{6}$$

In Fourier space, Green's function $\hat{G}^0_{ik}(\boldsymbol{\xi})$ and the Lippmann–Schwinger operator $\hat{\Gamma}^0_{ijkl}(\boldsymbol{\xi})$ read:

$$\hat{G}^0_{ik}(\boldsymbol{\xi}) = (C^0_{ijkl}\xi_j\xi_l)^{-1}$$
$$\hat{\Gamma}^0_{ijkl}(\boldsymbol{\xi}) = \frac{1}{4}(\hat{G}^0_{jk,il}(\boldsymbol{\xi}) + \hat{G}^0_{ik,jl}(\boldsymbol{\xi}) + \hat{G}^0_{jl,ki}(\boldsymbol{\xi}) + \hat{G}^0_{il,kj}(\boldsymbol{\xi})) \tag{7}$$

with the wave vector $\boldsymbol{\xi}$ gathering all the considered frequencies. To solve Equation (4) Moulinec and Suquet (1994, 1998) proposed an iterative solution procedure based on fixed point iterations computing $\boldsymbol{\tau}(\boldsymbol{x})$ in real space and solving Equation (6) in Fourier space. The best convergence behavior in terms of this basic fixed-point scheme is achieved by defining the reference material behavior $\mathbf{C}^0$ as arithmetic mean of the phase-wise material behavior. To avoid numerical resolution problems in this context, which are related to the Gibbs phenomenon (Gibbs, 1898), Willot (2015) suggested using a first-order finite difference approximation of the differential operator in Equation (7).

3. Model order reduction technique based on a reduced set of frequencies

To reduce the computational effort of solving the Lippmann–Schwinger equation in Fourier space (Equation (6)), Kochmann et al. (2019) proposed a MOR technique, which only considers a reduced set of frequencies. This method utilizes the fact that Green's operator and the polarization stress in Equation (6) are given in terms of a Fourier series. The accuracy of this representation depends on the number of considered frequencies. While the exactness of the approximation decreases with a lower number of considered frequencies, also the computational effort of solving the Lippmann–Schwinger equation in Fourier space is reduced. Accordingly, a reduced set of frequencies should decrease this computational effort, but still lead to a desired quality of the solution.

Besides the dependence on the number of used frequencies, the accuracy of this MOR method also depends on their choice. While Kochmann et al. (2019) suggested a fixed, radial sampling pattern, Gierden et al. (2021b) proposed to use a reduced set of frequencies adapted to the geometry of the microstructure. This new definition of sampling patterns significantly improves the quality of the results. Nevertheless, considering a nonlinear material behavior, the application of the strain-based sampling pattern S_ε leads to a further improvement of the calculated solution. In this context, the strain of the previous load step defines the sampling pattern for the next load step, as shown in Figure 1.

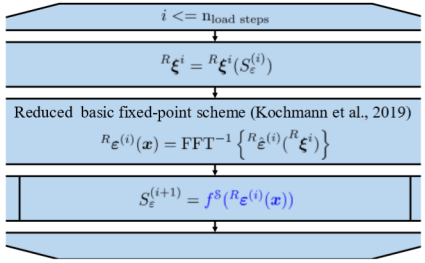

Fig. 1. Algorithm for adapting the sampling pattern S_g after each load step

Therefore, the norm of the strain field $\boldsymbol{\varepsilon}$ is transferred into Fourier space. To achieve a good approximation of this strain using a reduced set of frequencies, the frequencies with the highest amplitudes must be used. Similar to the geometrically adapted sampling pattern by Gierden et al. (2021b), the sampling pattern is thereby defined as consisting of a prescribed percentage of frequencies with the highest amplitudes needed to capture the norm of the strain. To further improve the accurateness of this method, the strain is first computed once, using the full set of frequencies. Figure 2 summarizes this algorithm to define the strain-based sampling pattern.

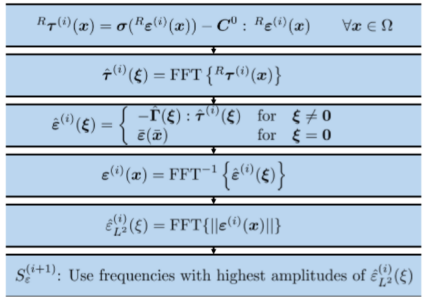

Fig. 2. Algorithm $f^S({}^R\varepsilon^{(i)}(x))$ to define the strain-based sampling pattern

As shown in Section 4, such a strain-based sampling pattern leads to significantly more accurate results compared to the fixed, radial S_f and geometrically adapted S_g sampling patterns.

4. Results and discussion

To compare the results of the simulation with different sampling pattern definitions, we consider a two-phase microstructure with elastic inclusions embedded in an

elasto-plastic matrix phase. Figure 3 shows the considered microstructure, material parameters, and prescribed macroscopic strain.

The prescribed strain is applied to the microstructure within 100 load steps. Figure 4 shows the resulting norm of the strain field and the related strain-based sampling pattern for four load steps. The strain field in the first load step is computed using the full set of frequencies. Considering the sampling patterns, the frequencies are rearranged on a squared grid with the lowest frequencies in the center and the highest frequencies at the edges. The frequencies highlighted in white correspond to the frequencies with the highest amplitudes in Fourier space needed to capture the norm of the strain field and are therefore taken into account within the simulation, while the frequencies highlighted in black are neglected.

The material behavior within the first 20 load steps is elastic. This results in a linear scaling of the present strain field within these load steps (see Figure 4, top row). Due to that, the sampling pattern does not change from load step 1 to 20 (see Figure 4, bottom row). After exceeding the yield stress within the matrix phase, the sampling pattern changes from step to step according to the elasto-plastic strain. Figure 4 shows for example norm of the elasto-plastic strain field and the sampling patterns for load step 30 and 100.

The resulting stress field σ_{xx} computed with the strain-based sampling pattern S_g is presented and compared to the reference solution, computed with the full set of frequencies, in Figure 5. The difference $\Delta\sigma_{xx}$ in the resulting stress field is defined as follows:

$$\Delta\sigma_{xx} = |\sigma_{xx}^{ref} - \sigma_{xx}|$$

In addition, Figure 5 shows the results computed with the same number of frequencies but with the geometrically adapted sampling pattern S_g. Considering $R = 0.8\%$ percent of frequencies, the difference in the stress field compared to the reference solution is significantly smaller for the solution with the newly defined strain-based sampling pattern compared to the solution with the geometrically adapted sampling pattern. This improvement particularly holds in the transition zone from matrix material to inclusion.

material constants

matrix

$\mu_{\mathrm{M}} = 1.0\,\mathrm{GPa}, \lambda_{\mathrm{M}} = 1.0\,\mathrm{GPa}$

$\sigma_{\mathrm{y0,M}} = 0.01\mathrm{GPa}, H_{\mathrm{M}} = 0.01\mathrm{GPa}$

inclusion

$\mu_{\mathrm{I}} = 2.0\,\mathrm{GPa}, \lambda_{\mathrm{I}} = 2.0\,\mathrm{GPa}$

macroscopic strain

$$\bar{\varepsilon} = \begin{pmatrix} 0.01 & 0.002 \\ 0.002 & -0.01 \end{pmatrix}$$

Fig. 3. Two-phase microstructure with several inclusions (white) embedded in a softer matrix material (black), material constants and prescribed macroscopic strain

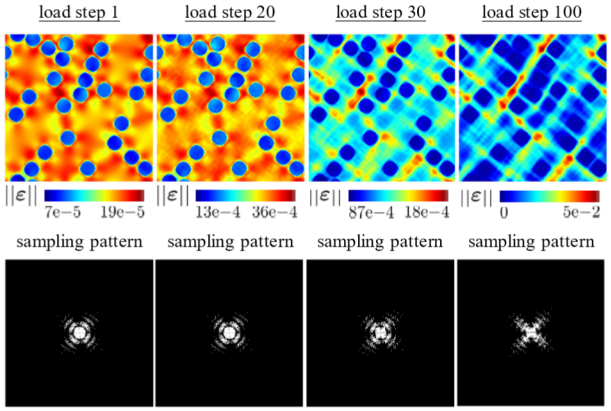

Fig. 4. Norm of the strain field and sampling patterns with the considered frequencies highlighted in white for load steps 1, 20, 30 and 100

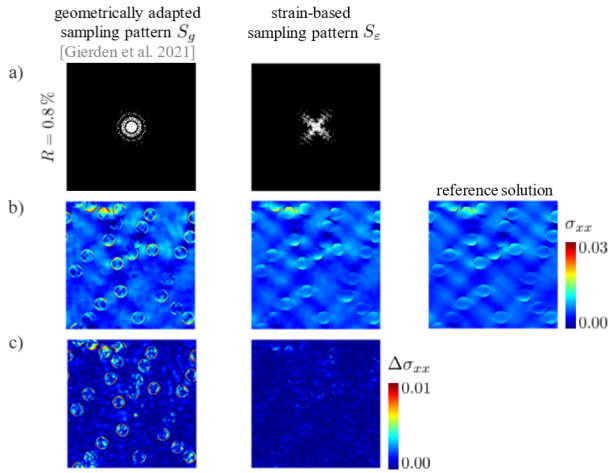

Fig. 5. Geometrically adapted vs. strain-based sampling pattern of the last load step (a), corresponding stress fields and reference solution (b), differences in the stress fields compared to the reference solution (c)

In addition, Figure 6 shows the relative macroscopic ($\bar{E}$) and microscopic error (E):

$$\bar{E} = \frac{\left\| \bar{\boldsymbol{\sigma}} - \bar{\boldsymbol{\sigma}}^{ref} \right\|}{\left\| \bar{\boldsymbol{\sigma}}^{ref} \right\|}$$

$$E = \frac{1}{n} \sum_{n} \frac{\left\| \boldsymbol{\sigma}(n) - \boldsymbol{\sigma}^{ref}(n) \right\|}{\left\| \boldsymbol{\sigma}^{ref}(n) \right\|}$$

for the fixed, the geometrically adapted, as well as the strain-based sampling pattern. Here, $\bar{\boldsymbol{\sigma}}$ is the overall averaged stress, n is the number of grid points, and the superscript *ref* refers to the solution computed with the full set of frequencies. These errors are always the lowest for the strain-based sampling pattern. Considering a highly reduced set of frequencies, for example 1.5% of frequencies, the microscopic error for the fixed sampling pattern goes up to 80% , while this error is 14% for the geometrically adapted sampling pattern, but only 4% for the strain-based sampling pattern. Similar results are gained for the macroscopic error. For the fixed sampling pattern, the error goes up to 34%, for the geometrically adapted sampling pattern the error is reduced to 1.8%, but for the strain-based sampling pattern, the error is even reduced to only 0.2%. The speed-up factor for all these simulations is about 5 compared to the simulation with the full set of frequencies and similar for all three different sampling patterns, see Figure 7. Even though the sampling pattern is redefined after each load step for the strain-based sampling pattern, the computational effort is not significantly higher since a better convergence behavior is observed for solving the Lippmann–Schwinger equation within one load step.

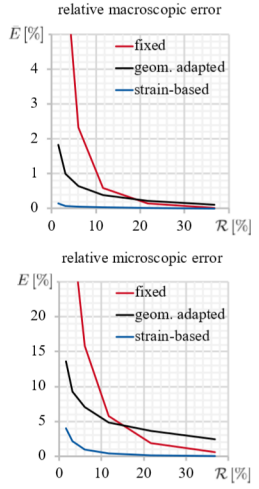

Fig. 6. Relative macroscopic error E and relative microscopic error $\bar{E}$ for the solution with the fixed, geometrically adapted and strain-based sampling pattern

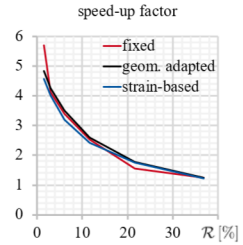

Fig. 7. Speed-up factor for the simulation with the fixed, geometrically adapted and strain-based sampling pattern

5. Conclusions and outlook

We presented a new approach to defining a strain-based reduced set of frequencies for a reduced FFT-based microstructure simulation. Considering a nonlinear material behavior, this approach utilizes the strain of the last load step to define the sampling pattern for the next load step. Compared to the results with the fixed and geometrically adapted sampling patterns, the new approach leads to more accurate results without increasing the computational effort of the reduced fixed-point scheme.

Since the MOR technique only reduces the computational costs for solving the Lippmann–Schwinger equation in Fourier space, there is no speed-up for the evaluation of the constitutive behavior. To decrease the related computational effort, a coupling of the MOR technique with a clustered microstructure (Liu et al., 2016; Waimann et al., 2021; Wulfinghoff et al., 2018) is currently under investigation. In further studies, the basic fixed-point scheme used will additionally be replaced by more efficient solvers, such as a Newton Krylov solver (Brisard & Dormieux, 2010; Zeman et al., 2010), to further improve the computational performance.

Acknowledgements

The authors gratefully acknowledge the financial support of the research work by the German Research Foundation (DFG, Deutsche Forschungsgemeinschaft) within the transregional Collaborative Research Center SFB/TRR 136, project number 223500200, subproject M03. In addition, Stefanie Reese gratefully acknowledges the financial support of the research work by the German Research Foundation (DFG, Deutsche Forschungsgemein-schaft) within the transregional Collaborative Research Center SFB/TRR 280, project number 417002380, subproject A01 and the project "Model order reduction in space and parameter dimension - towards damage-based modeling of polymorphic uncertainty in the context of robustness and reliability", project number 312911604, from the priority program SPP 1886.

References

Brisard, S., & Dormieux, L. (2010). FFT-based methods for the mechanics of composites: A general variational framework. *Computational Materials Science*, *49*(3), 663–671. https://doi.org/10.1016/j.commatsci.2010.06.009.

Garcia-Cardona, C., Lebensohn, R., & Anghel, M. (2017). Parameter estimation in a thermoelastic composite problem via adjoint formulation and model reduction. *International Journal for Numerical Methods in Engineering*, *112*(6), 578–600. https://doi.org/10.1002/nme.5530.

Gibbs, J.W. (1898). Fourier's series. *Nature*, *59*(1522), 200.

Gierden, C., Kochmann, J., Waimann, J., Kinner-Becker, T., Sölter, J., Svendsen, B., & Reese, S. (2021a). Efficient two-scale FE-FFT-based mechanical process simulation of elasto-viscoplastic polycrystals at finite strains. *Computer Methods in Applied Mechanics and Engineering*, *374*, 113566. https://doi.org/10.1016/j.cma.2020.113566.

Gierden, C., Waimann, J., Svendsen, B., & Reese, S. (2021b). A geometrically adapted reduced set of frequencies for a FFT-based microstructure simulation. *Cornell University, arXiv.org*, arXiv:2103.10203.

Hashin, Z., & Shtrikman, S. (1962). On some variational principles in anisotropic and nonhomogeneous elasticity. *Journal of the Mechanics and Physics of Solids*, *10*(4), 335–342. https://doi.org/10.1016/0022-5096(62)90004-2.

Kochmann, J., Wulfinghoff, S., Reese, S., Mianroodi, J.R., & Svendsen, B. (2016). Two-scale FE–FFT- and phase-field-based computational modeling of bulk microstructural evolution and macroscopic material behavior. *Computer Methods in Applied Mechanics and Engineering*, *305*, 89–110. https://doi.org/10.1016/j.cma.2016.03.001.

Kochmann, J., Wulfinghoff, S., Ehle, L., Mayer, J., Svendsen, B., & Reese, S. (2018). Efficient and accurate two-scale FE-FFT-based prediction of the effective material behavior of elasto-viscoplastic polycrystals. *Computational Mechanics*, *61*(6), 751–764. https://doi.org/10.1007/s00466-017-1476-2.

Kochmann, J., Manjunatha, K., Gierden, C., Wulfinghoff, S., Svendsen, B., & Reese, S. (2019). A simple and flexible model order reduction method for FFT-based homogenization problems using a sparse sampling technique. *Computer Methods in Applied Mechanics and Engineering*, *347*, 622–638. https://doi.org/10.1016/j.cma.2018.11.032.

Kröner, E. (1959). Allgemeine Kontinuumstheorie der Versetzungen und Eigenspannungen. *Archive for Rational Mechanics and Analysis*, *4*(1), 273–334.

Liu, Z., Bessa, M.A., & Liu, W.K. (2016). Self-consistent clustering analysis: an efficient multi-scale scheme for inelastic heterogeneous materials. *Computer Methods in Applied Mechanics and Engineering*, *306*, 319–341. https://doi.org/10.1016/j.cma.2016.04.004.

Moulinec, H., & Suquet, P. (1994). A fast numerical method for computing the linear and nonlinear mechanical properties of composites. *Comptes Rendus de l'Académie des Sciences. Série II. Mécanique, physique, chimie, astronomie*, *318*, 1417–1423.

Moulinec, H. & Suquet, P. (1998). A numerical method for computing the overall response of nonlinear composites with complex microstructure. *Computer Methods in Applied Mechanics and Engineering*, *157*(1–2), 69–94. https://doi.org/10.1016/S0045-7825(97)00218-1.

Smit, R.J.M., Brekelmans, W.A.M., & Meijer, H.E.H. (1998). Prediction of the mechanical behavior of nonlinear heterogeneous systems by multi-level finite element modeling. *Computer Methods in Applied Mechanics and Engineering*, *155*, 181–192. https://doi.org/10.1016/S0045-7825(97)00139-4.

Spahn, J., Andrä, H., Kabel, M., & Müller, R. (2014). A multiscale approach for modeling progressive damage of composite materials using fast Fourier transforms. *Computer Methods in Applied Mechanics and Engineering*, *268*, 871–883. https://doi.org/10.1016/j.cma.2013.10.017.

Vondřejc, J., Liu, D., Ladecký, M., & Matthies, H.G. (2020). FFT-based homogenisation accelerated by low-rank tensor approximations. *Computer Methods in Applied Mechanics and Engineering*, *364*, 112890. https://doi.org/10.1016/j.cma.2020.112890.

Waimann, J., Gierden, C., Schmidt, A., Svendsen, B., & Reese, S. (2021). Microstructure simulation using self-consistent clustering analysis. *PAMM. Proceedings in Aplied Mathematics and Mechanics*, *20*(1), e202000263. https://doi.org/10.1002/pamm.202000263.

Willis, J.R. (1981). Variational and related methods for the overall properties of composites. In C.-S. Yih (Ed.), *Advances in applied mechanics* (Vol. 21, pp. 1–78). Elsevier. https://doi.org/10.1016/S0065-2156(08)70330-2.

Willot, F. (2015). Fourier-based schemes for computing the mechanical response of composites with accurate local fields. *Comptes Rendus Mécanique*, *343*(3), 232–245. https://doi.org/10.1016/j.crme.2014.12.005.

Wulfinghoff, S., Cavaliere, F., & Reese, S. (2018). Model order reduction of nonlinear homogenization problems using a Hashin–Shtrikman type finite element method. *Computer Methods in Applied Mechanics and Engineering*, *330*, 149–179. https://doi.org/10.1016/j.cma.2017.10.019.

Zeman, J., Vondřejc, J., Novák, J., & Marek, I. (2010). Accelerating a FFT-based solver for numerical homogenization of periodic media by conjugate gradients. *Journal of Computational Physics*, *229*(21), 8065–8071. https://doi.org/10.1016/j.jcp.2010.07.010.